A Operator-Induced Geometry of Node Role Evaluation ψ

Let $G = (\mathcal{V}, E)$ denote a connectome graph, where each node $v \in \mathcal{V}$ is characterized by multiple structural descriptors capturing connectivity at different scales. In this work, we consider a node-role evaluation function

$$\boldsymbol{\psi} : \mathcal{V} \to \{1 \cdots B\}, \tag{4}$$

which assigns each node to one of B structural blocks based on aggregated structural evidence. Sample $\boldsymbol{\psi}$ values using connectomes with 129 nodes from the HCP connectome dataset is shown in Fig. 7.

Local and global structural evidence. For each node $v \in \mathcal{V}$, let

$$x(v) \in \mathbb{R}^+ \quad \text{and} \quad y(v) \in \mathbb{R}^+$$

denote normalized local and global structural measures, respectively. Typical choices include local degree or clustering coefficients for $x(v)$, and betweenness centrality, participation coefficient, or module-level influence for $y(v)$. The function $\boldsymbol{\psi}$ is realized by aggregating $(x(v), y(v))$ through a scalar scoring functional $f : \mathbb{R}^2 \to \mathbb{R}$, followed by discretization into blocks.

Aggregation operators as implicit geometric priors. Fig. 8 visualizes the induced partitioning of the (x, y)-plane under different choices of f, illustrating that the aggregation rule itself imposes a strong geometric bias on node-role assignments.

Average aggregation (see Fig. 8).

$$f_{\text{avg}}(x, y) = \tfrac{1}{2}(x + y). \tag{5}$$

This choice induces smooth, approximately linear decision boundaries and implicitly assumes commensurability between local and global evidence. While appropriate for homogeneous connectomes, it tends to blur structurally distinct roles such as connector hubs and provincial hubs.

Difference-based aggregation (see Fig. 8).

$$f_{\text{diff}}(x, y) = |x - y|. \tag{6}$$

This operator emphasizes structural imbalance, highlighting nodes whose local and global roles diverge. Such nodes often correspond to transitional or anomalous regions, making this aggregation more suitable for diagnostics than stable role assignment.

Maximum aggregation (see Fig. 8).

$$f_{\max}(x, y) = \max(x, y). \tag{7}$$

Here, node roles are dominated by the strongest structural signal. The resulting partitioning exhibits sharp, piecewise boundaries, favoring highly influential hubs but remaining sensitive to noise in extreme values.

Minimum aggregation (see Fig. 8).

$$f_{\min}(x, y) = \min(x, y). \tag{8}$$

This conservative operator assigns high rank only to nodes that are simultaneously strong in both local and global senses. While robust, it systematically penalizes asymmetric yet functionally critical nodes such as inter-modular connectors.

Product aggregation.

$$f_{\text{prod}}(x, y) = x \cdot y. \tag{9}$$

Product aggregation introduces a nonlinear coupling between structural scales, leading to curved decision boundaries and a non-Euclidean geometry in the role space. This behavior naturally captures hierarchical organization in connectomes, where node importance emerges from the joint reinforcement of local specialization and global integration.

Implications for connectome modeling. These visualizations demonstrate that $\boldsymbol{\psi}$ is not a neutral mapping but an operator-induced geometric embedding. Different aggregation rules encode distinct assumptions about robustness, dominance, and multiscale interaction, which in turn shape block formation, inter-block diffusion, and downstream generative dynamics. This observation motivates our geometry-aware design of $\boldsymbol{\psi}$, ensuring that node-role assignments faithfully reflect the hierarchical and multiscale structure of real connectomes.

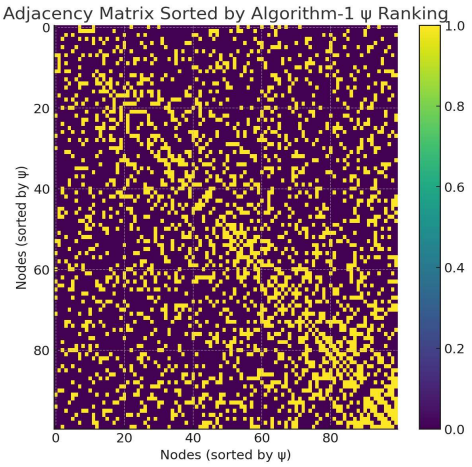

Figure 7: Sample node-wise ψ values (using Algorithm 1) of HCP connectome data with 129 nodes from `BrainGraph.org`.

Table 2: Baseline comparison on HCP-234 with 1064 samples from HCP connectome dataset (from `BrainGraph.org`).

Model	MSE ↓	Pearson ↑	Spec. Dist ↓	NMI (Blocks) ↑	AUPRC↑
DiGress [51]	0.021	0.86	0.13	0.82	0.79
GraphDDPM [16]	0.028	0.82	0.16	0.78	0.75
EDP-GNN [52]	0.032	0.79	0.18	0.75	0.72
GDSS [22]	0.037	0.77	0.21	0.71	0.69
MoFlow [58]	0.042	0.72	0.25	0.62	0.61
Erdos-Renyi [10]	0.098	0.09	0.93	0.05	0.12
Ours	**0.019**	**0.88**	**0.11**	**0.85**	**0.82**

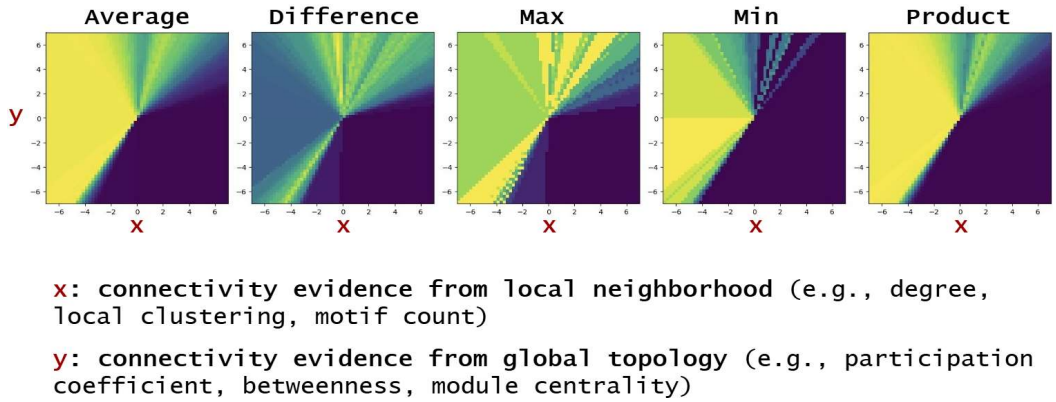

Figure 8: Induced partitioning of the local–global structural evidence space under different node-role aggregation operators $f(x, y)$. Each operator defines a distinct geometry for the node-role evaluation function ψ, resulting in qualitatively different block assignments in connectome graphs. This uses OASIS-3 data from `BrainGraph.org`.

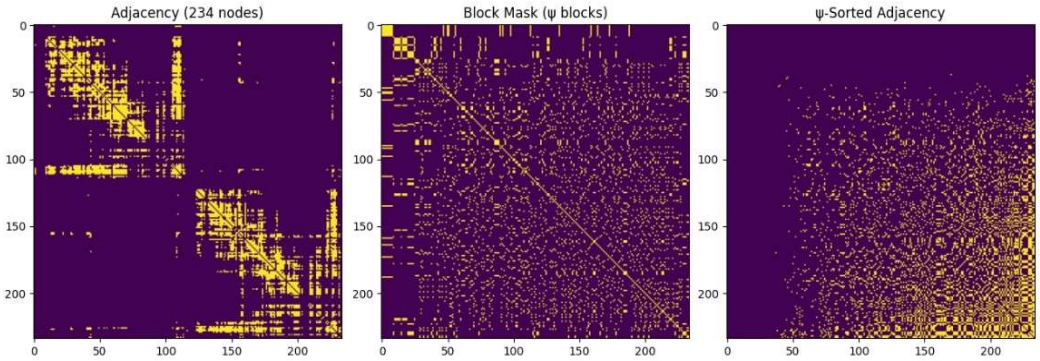

Figure 9: 1. Original HCP Connectome sample with 234 nodes; 2. Corresponding ψ-values calculated using Algorithm 1; and 3. Sorted ψ values based on adjacency. Here, we used HCP Connectome samples with 234 nodes from `BrainGraph.org`.

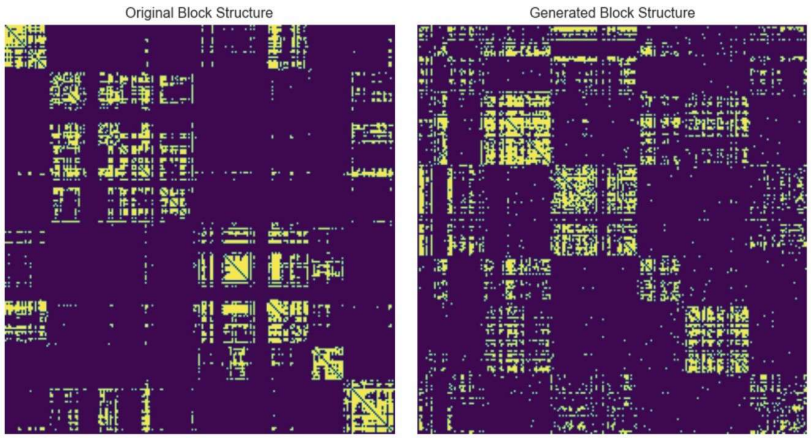

Figure 10: Generated block structure inside connectomes using proposed Neuro-PARSDiff. Here, we used HCP Connectome samples with 234 nodes from `BrainGraph.org`.

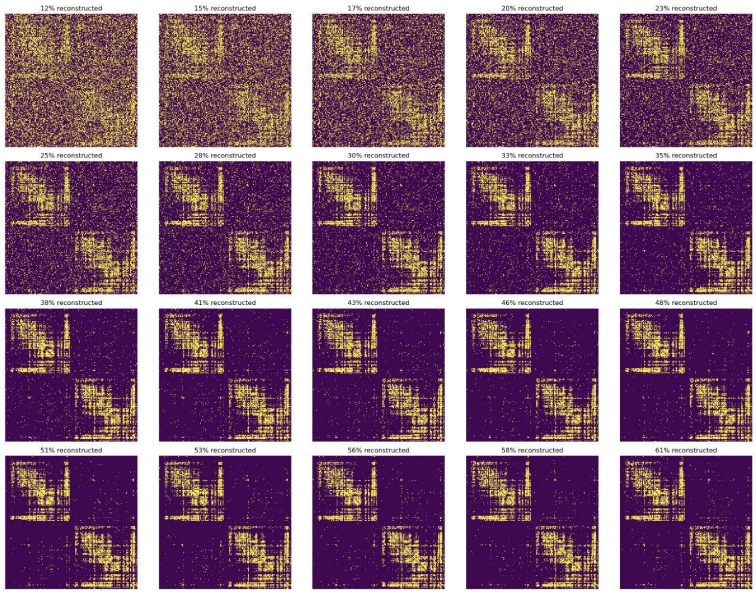

Figure 11: Gradual reconstruction of connectomes with 234 nodes (from 12% to 61%) using the proposed Neuro-PARSDiff. Here, we used HCP Connectome samples with 234 nodes from `BrainGraph.org`.

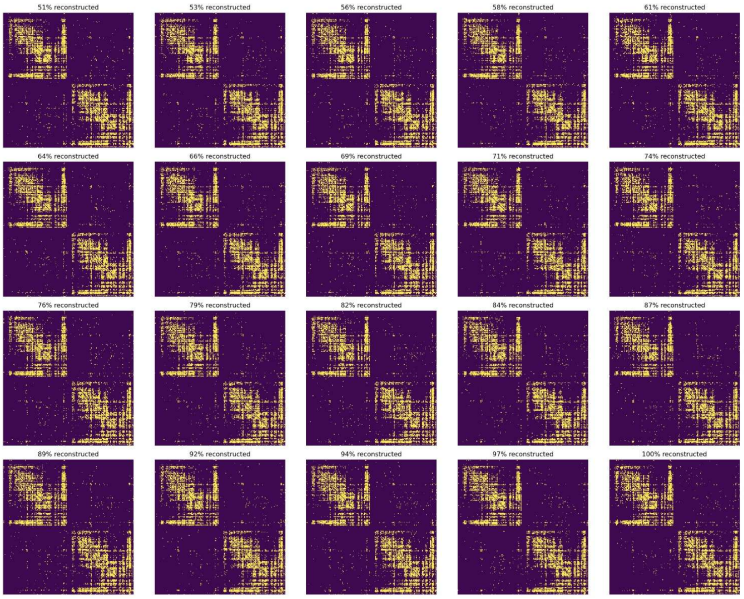

Figure 12: Gradual reconstruction of connectomes with 234 nodes (from 51% to 100%) using the proposed Neuro-PARSDiff. Here, we used HCP Connectome samples with 234 nodes from `BrainGraph.org`.

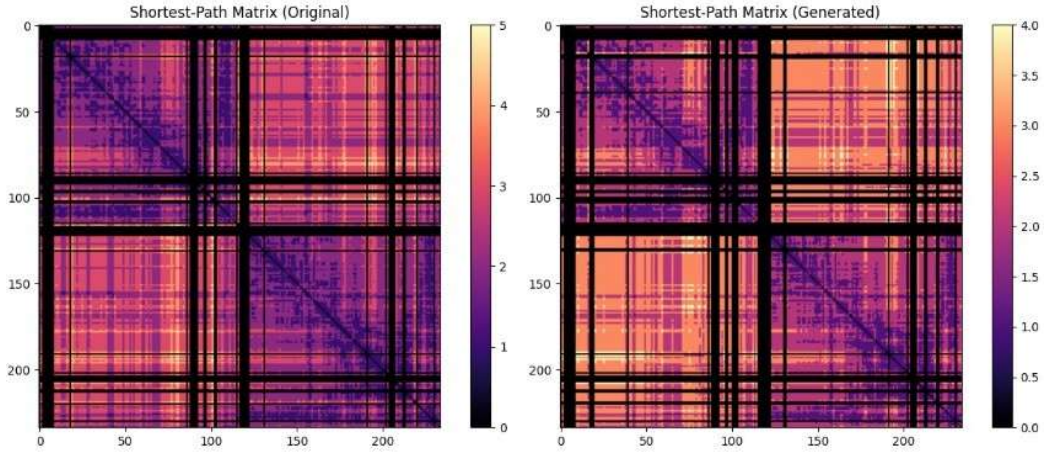

Figure 13: Comparison between the shortest path matrices of the original and final generated connectome with 234 nodes using the proposed Neuro-PARSDiff. Here, we used HCP Connectome samples with 234 nodes from `BrainGraph.org`.

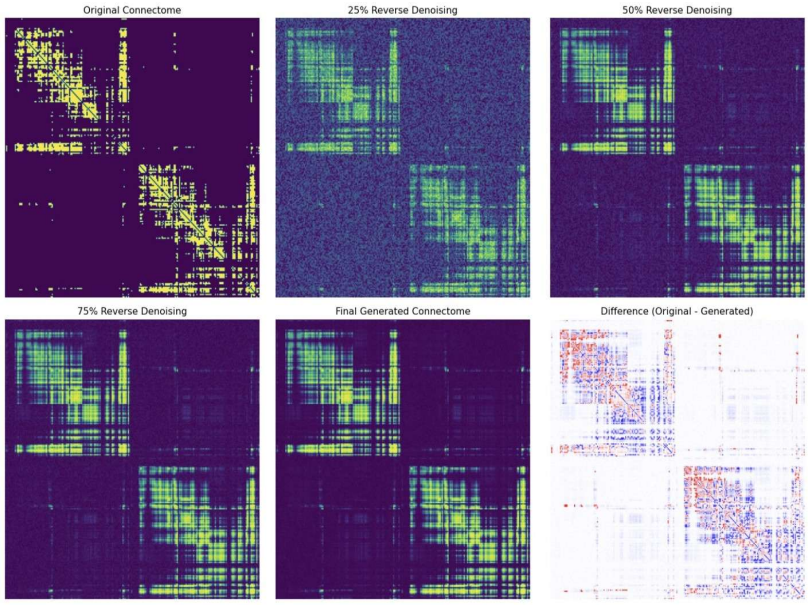

Figure 14: Original and final generated connectome with 463 nodes using the proposed Neuro-PARSDiff. Here, we used HCP Connectome samples with 463 nodes from `BrainGraph.org`.

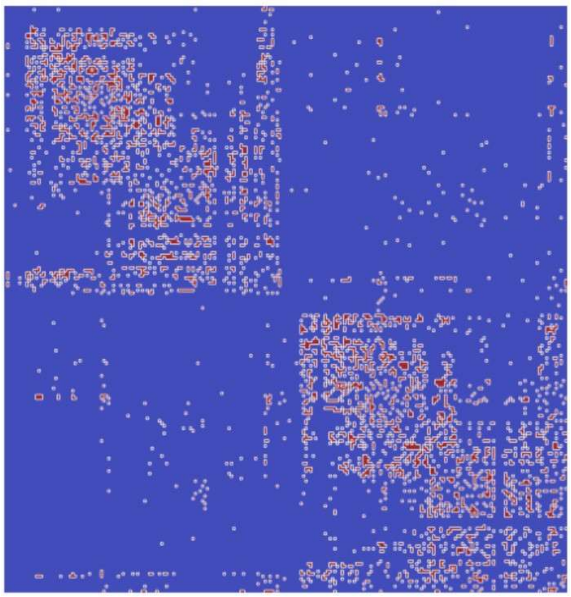

Figure 15: Difference between the original and the generated connectome using the proposed Neuro-PARSDiff (better visualization). Here, we used HCP Connectome samples with 463 nodes from `BrainGraph.org`.

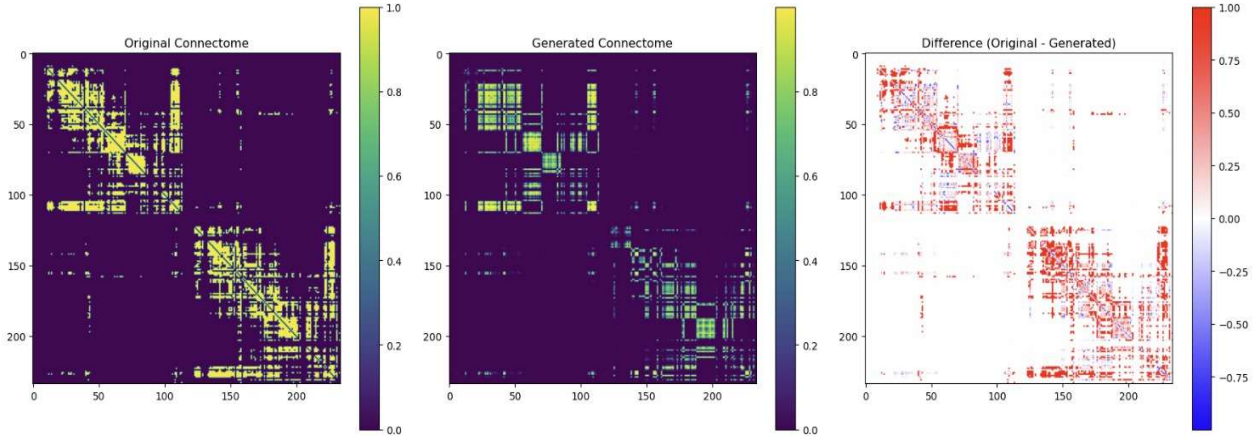

Figure 16: Comparison between the original connectome adjacency matrix (left), the generated connectome produced by the proposed role-aware model (middle), and their difference (right). The generated connectome preserves the global block structure induced by the node-role evaluation function ψ, while residual errors concentrate around inter-module connections and connector hubs, reflecting regions of high structural variability. This directly supports our claim: role-aware generative modeling yields faithful reconstruction of connectome topology while exposing biologically meaningful uncertainty at module interfaces. Here, we used HCP Connectome samples with 234 nodes from `BrainGraph.org`.

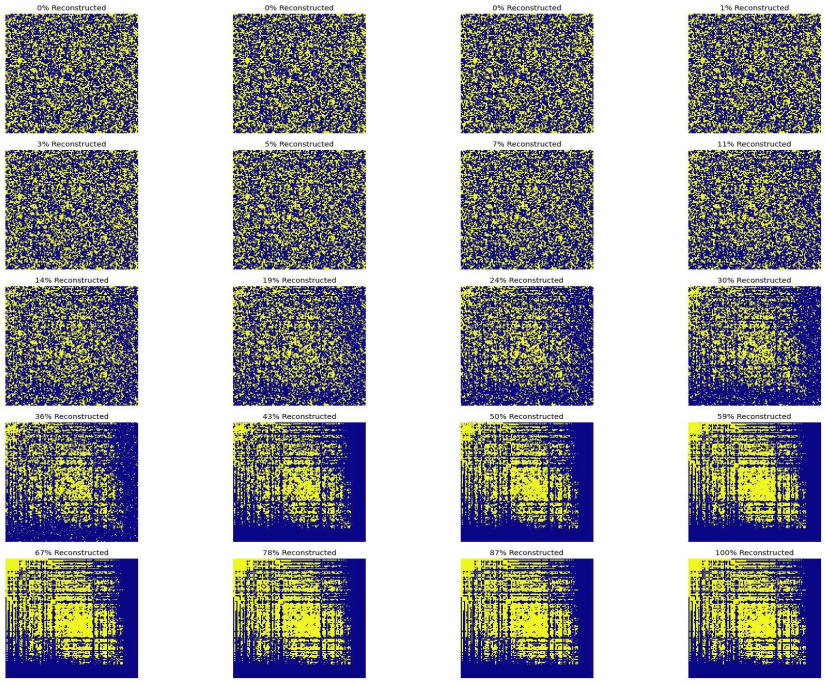

Figure 17: Gradual reconstruction of sample OASIS-3 connectome (between 3% and 100%). Here, we used OASIS-3 samples with 1058 nodes from `BrainGraph.org`.

B Industrial Impact of Neuro-PARSDiff

Modern neuroscience and healthcare industries increasingly rely on large-scale brain connectivity data, yet face a fundamental bottleneck: high-quality connectome data are expensive to acquire, limited in availability, and constrained by strict privacy and ethical requirements. Neuro-PARSDiff addresses this challenge by enabling structure-faithful, role-aware generative modeling of brain connectomes, transforming connectome analysis from a data-limited process into a scalable, model-driven workflow.

B.1 Scalable and privacy-preserving neurodata generation.

In clinical practice and industrial research, acquiring connectome data requires specialized imaging infrastructure, long acquisition times, and careful handling of sensitive patient information. Neuro-PARSDiff enables the generation of statistically consistent and biologically plausible connectomes conditioned on learned structural roles, allowing hospitals, medical AI vendors, and pharmaceutical partners to augment limited datasets without exposing raw patient data. This capability significantly reduces both data acquisition costs and regulatory barriers, facilitating broader adoption of connectome-driven AI systems.

B.2 Accelerating early detection and precision neurology.

Many neurodegenerative and neurodevelopmental disorders manifest as subtle and distributed changes in network organization long before observable clinical symptoms. By explicitly modeling node roles, block structure, and multiscale interactions, Neuro-PARSDiff supports the simulation of disease-progression trajectories and the identification of structurally meaningful deviations from healthy baselines. This enables industrial diagnostic platforms to develop early-warning systems for conditions such as Alzheimer's disease, Parkinson's disease, and autism spectrum disorders, thereby advancing precision neurology and personalized intervention strategies.

B.3 Robust AI development and validation.

Industrial deployment of neuro-AI systems requires models that generalize reliably across populations, imaging protocols, and clinical settings. Neuro-PARSDiff facilitates systematic generation of diverse yet structurally coherent connectomes, enabling large-scale robustness testing, bias analysis, and out-of-distribution evaluation. These capabilities are critical for meeting emerging regulatory standards and ensuring safe, trustworthy deployment of AI-driven neurological tools.

B.4 Integration with digital twin technologies.

The growing adoption of digital twins in healthcare demands generative models that preserve hierarchical modularity, hub organization, and inter-module coupling. Neuro-PARSDiff naturally aligns with this paradigm by producing connectomes that retain core structural properties essential for simulating brain dynamics. Industrial platforms can integrate Neuro-PARSDiff into digital-twin pipelines for treatment simulation, intervention planning, and

longitudinal monitoring, supporting data-driven clinical decision-making.

B.5 Reducing development cost and time-to-market.

From an industrial perspective, Neuro-PARSDiff reduces reliance on repeated and costly neuroimaging studies by enabling realistic synthetic data generation at scale. This results in shorter development cycles and lower operational costs for neurotechnology startups, medical device companies, and pharmaceutical collaborations, accelerating time-to-market for connectome-based AI products.

B.6 Broader industrial applicability.

While Neuro-PARSDiff is designed for brain connectomes, its underlying principles of role-aware and block-structured generative modeling extend to other complex network domains, including brain–computer interfaces, cognitive robotics, and large-scale biological networks. This generality enhances its long-term industrial relevance and positions Neuro-PARSDiff as a foundational tool for network-centric AI systems.

Summary. Overall, Neuro-PARSDiff elevates connectome generation from an academic exercise to a deployable industrial capability. By combining structural realism, scalability, and privacy awareness, it enables the development of robust, trustworthy, and clinically relevant neuro-AI systems, supporting earlier diagnosis, improved treatment planning, and accelerated innovation in brain-inspired technologies.

C Used Baseline Metrics

C.1 Mean Squared Error (MSE)

The mean squared error between the original connectome $\mathbf{A}$ and the generated connectome $\hat{\mathbf{A}}$ is defined as

$$\mathrm{MSE}(\mathbf{A}, \hat{\mathbf{A}}) = \frac{1}{N^2} \sum_{i=1}^{N} \sum_{j=1}^{N} \left(A_{ij} - \hat{A}_{ij} \right)^2. \tag{10}$$

□

C.2 Peak Signal-to-Noise Ratio (PSNR)

Assuming connectome weights are normalized to $[0, 1]$, the PSNR is defined as

$$\mathrm{PSNR}(\mathbf{A}, \hat{\mathbf{A}}) = 10 \log_{10} \left(\frac{1}{\mathrm{MSE}(\mathbf{A}, \hat{\mathbf{A}})} \right). \tag{11}$$

□

C.3 Pearson Correlation (CORR)

Let $\mathrm{vec}(\cdot)$ denote vectorization of the upper-triangular entries of a matrix. The Pearson correlation between $\mathbf{A}$ and $\hat{\mathbf{A}}$ is defined as

$$\mathrm{CORR}(\mathbf{A}, \hat{\mathbf{A}}) = \frac{\mathrm{cov}\left(\mathrm{vec}(\mathbf{A}), \mathrm{vec}(\hat{\mathbf{A}}) \right)}{\sigma_{\mathbf{A}} \sigma_{\hat{\mathbf{A}}}}, \tag{12}$$

where $\sigma_{\mathbf{A}}$ and $\sigma_{\hat{\mathbf{A}}}$ are standard deviations. □

C.4 Normalized Mutual Information (NMI)

We compute NMI between discretized versions of $\mathbf{A}$ and $\hat{\mathbf{A}}$ as

$$\mathrm{NMI}(\mathbf{A}, \hat{\mathbf{A}}) = \frac{2\, I(\mathbf{A}; \hat{\mathbf{A}})}{H(\mathbf{A}) + H(\hat{\mathbf{A}})}, \tag{13}$$

where $I(\cdot;\cdot)$ denotes mutual information and $H(\cdot)$ denotes Shannon entropy. □

C.5 Spectral Distance (SPEC)

Let $\mathbf{L} = \mathbf{D} - \mathbf{A}$ and $\hat{\mathbf{L}} = \hat{\mathbf{D}} - \hat{\mathbf{A}}$ denote the graph Laplacians of the original and generated connectomes, with eigenvalues $\{\lambda_k\}_{k=1}^{N}$ and $\{\hat{\lambda}_k\}_{k=1}^{N}$, respectively. The spectral distance is defined as

$$\mathrm{SPEC}(\mathbf{A}, \hat{\mathbf{A}}) = \frac{1}{N} \sum_{k=1}^{N} \left| \lambda_k - \hat{\lambda}_k \right|. \tag{14}$$

□

Together, these metrics jointly evaluate local edge fidelity, global structural alignment, nonlinear information preservation, and spectral topology, providing a comprehensive assessment of generative quality in Neuro-PARSDiff.

Received 20 February 2007; revised 12 March 2009; accepted 5 June 2009